AMERICAN METEOROLOGICAL SOCIETY

Journal of Climate

EARLY ONLINE RELEASE

The DOI for this manuscript is doi: 10.1175/JCLI-D-13-00780.1

Sensitivity of Tropical Cyclone Rainfall to Idealized Global Scale Forcings

GABRIELE VILLARINI[1], DAVID A. LAVERS[1], ENRICO SCOCCIMARRO[2,3], MING ZHAO[4], MICHAEL F. WEHNER[5], GABRIEL A. VECCHI[4], THOMAS R. KNUTSON[4] AND KEVIN A. REED[6]

[1] IIHR-Hydroscience & Engineering, The University of Iowa, Iowa City, Iowa, USA

[2] Istituto Nazionale di Geofisica e Vulcanologia (INGV), Bologna, Italy

[3] Centro Euro-Mediterraneo sui i Cambiamenti Climatici (CMCC), Lecce, Italy

[4] NOAA/Geophysical Fluid Dynamics Laboratory, Princeton, New Jersey

[5] Lawrence Berkeley National Laboratory, Berkeley, California, USA

[6] National Center for Atmospheric Research, Boulder, Colorado, USA

Manuscript submitted to

Journal of Climate

18 December 2013

revised February 2014

Corresponding author address:

Gabriele Villarini, IIHR-Hydroscience & Engineering, The University of Iowa, Iowa City, IA 52242. E-mail: gabriele-villarini@uiowa.edu

ABSTRACT

Heavy rainfall and flooding associated with tropical cyclones (TCs) are responsible for a large number of fatalities and economic damage worldwide. Despite their large socio-economic impacts, research into heavy rainfall and flooding associated with TCs has received limited attention to date, and still represents a major challenge. Our capability to adapt to future changes in heavy rainfall and flooding associated with TCs is inextricably linked to and informed by our understanding of the sensitivity of TC rainfall to likely future forcing mechanisms. Here we use a set of idealized high-resolution atmospheric model experiments produced as part of the U.S. CLIVAR Hurricane Working Group activity to examine TC response to idealized global-scale perturbations: the doubling of CO_2, uniform 2K increases in global sea surface temperature (SST), and their combined impact. As a preliminary but key step, daily rainfall patterns of composite TCs within climate model outputs are first compared and contrasted to the observational records. To assess similarities and differences across different regions in response to the warming scenarios, analyses are performed at the global and hemispheric scales and in six global TC ocean basins. The results indicate a reduction in TC daily precipitation rates in the doubling CO_2 scenario (on the order of 5% globally), and an increase in TC rainfall rates associated with a uniform increase of 2K in SST (both alone and in combination with CO_2 doubling; on the order of 10-20% globally).

1. INTRODUCTION

Every year, tropical cyclones (TCs) are responsible for a large number of fatalities and vast economic damages (e.g., Rappaport 2000, Pielke et al. 2008, Zhang et al. 2009, Jonkman et al. 2009, Czajkowski et al. 2011, 2013, Mendelsohn et al. 2012, Peduzzi et al. 2012). To compound these TC hazards, over the last few decades there has been an increase in population and infrastructure in global coastal regions resulting in increased TC-related damages (e.g., Mendelsohn et al. 2012, Peduzzi et al. 2012); this demographic change is acting in addition to the TC changes projected to occur as a result of climate change.

Although heavy rainfall is a major hazard associated with TCs, few studies have examined the rainfall patterns associated with these storms. A recent analysis of observations found that over the period 1994–2008 TC-related heavy rainfall events in the United States occurred over twice as often as the long-term average (Kunkel et al. 2010). Using satellite-based estimates of rainfall, Lau and Zhou (2012) point to an increase in north Atlantic TC rainfall over the period 1988-2007. At the same time, they also identified a decrease in TC rainfall in the north Pacific. Over China, Ren et al. (2006) found decreasing trends in both TC total precipitation and frequency of torrential rain, while Ying et al. (2011) found increasing trends in the intensity of tropical cyclone precipitation at some locations over southeast China. Based on climate model outputs, Knutson and Tuleya (2004) found a tendency for larger near-storm precipitation rates in TCs in CO_2 warming scenarios. In a review of TC/climate change studies, Knutson et al. (2010) found seven studies reporting an increase in TC-related rainfall (various metrics) under climate warming scenarios and no studies with decreases. Overall, TC-related rainfall rates are projected to increase on the order of 20% within 100km from the storm center for the late 21st century (Knutson et al. 2010). More recently, Knutson et al. (2013) used a range of global climate

models (GCMs), including outputs from climate models produced under phase 5 of the Coupled Model Intercomparison Project (CMIP5; Taylor et al. 2012), and found an increase in the average precipitation rate in north Atlantic TCs of about 10%, rising to over 20% within 100km of the storm center. Because of the observed and projected changes in TC rainfall and especially because of their large socio-economic effects, it is essential to evaluate TC rainfall patterns under warming scenarios.

The main goals of this study are to undertake a global scale analysis in six TC basins to analyse possible changes in TC rainfall under different warming scenarios using GCM runs. The research questions we will address are:

1) How well can GCMs reproduce the TC rainfall structure present in the observational records? Despite the simplicity of the question, very few studies have examined the capability of GCMs in reproducing the rainfall characteristics compared to the observational records.
2) What are the possible changes in TC rainfall that can be expected under different idealized warming scenarios? We will be able to address this question using a series of idealized experiments conducted in support of the U.S. CLIVAR – Hurricane and Climate Working Group.

The analyses will leverage on three state-of-the-art atmospheric models, and examine the changes in TC rainfall structure and magnitude in six TC genesis basins under three warming scenarios: (1) a doubling of CO_2 in the atmosphere with no change in SST, (2) a uniform 2K rise in global SST, and (3) a doubling of CO_2 plus a uniform 2K rise in SST. The expectation prior to performing the analyses is for a decrease in TC rainfall under the CO_2-doubling experiment and for an increase associated with the global increase in SST. It is more difficult to know a priori

what to expect from a combination of changes in both CO_2 and SST because of the potentially opposite effects associated with the changes in these two forcings. One of the main objectives of the U.S. CLIVAR working group, and these experiments, is to quantify changes in tropical cyclone characteristics in a warming climate.

This paper is organized as follows. The next section contains a description of the data, methods and models used. Section 3 presents the results, and is followed by Section 4, in which we summarize the main points of this study.

2. DATA AND METHODS

Six TC genesis basins were used in this analysis, four in the northern hemisphere (north Atlantic (NA), eastern north Pacific (EP), western north Pacific (WP), north Indian (NI)) and two in the southern hemisphere (south Indian (SI) and southern Pacific (SP)). The delineation of these basins is the same as the one used in Camargo et al. (2005), with the only exception that we combine their Australian and south Pacific basins into the southern Pacific basin, which extends eastward from 110W longitude, in order to have a larger storm sample. We also perform analyses at the global and hemispheric scales.

Observed TC tracks were taken from the International Best Track Archive for Climate Stewardship (IBTrACS v03r04; Knapp et al. 2010). It represents a unified database of global TC tracks, including data from numerous TC forecast centers around the world and other sources. The IBTrACS includes the latitude and longitude of the center of circulation of the recorded storms, maximum sustained wind and minimum central pressure every six hours during the storms' lifetime. Here we focus on the period 1997-2012 because it matches the period for which relatively high quality daily rainfall data are available globally.

Rainfall data are available over the period 1997-2012 through the Global Precipitation Climatology Project (GPCP; Huffman et al. 2001). This dataset provides global rainfall at the daily scale with a 1°×1° resolution. GPCP is obtained by merging different satellite-based rainfall estimates (in particular within and outside the latitude band 40° north-south) and rain gage data. Here GPCP is used as reference dataset for the comparison with modelled data. It is worth keeping in mind, though, that these are rainfall estimates based on satellite data, and not direct measurements of rainfall. Our assumption is that the uncertainties associated with this product are much smaller than what we would expect from modelled rainfall data.

These observational records will be used to evaluate the capability of three climate models in reproducing the rainfall characteristics associated with TCs. In this study we will use outputs from the Geophysical Fluid Dynamics Laboratory (GFDL) High Resolution Atmospheric Model (HiRAM), the Centro Euro-Mediterraneo per i Cambiamenti Climatici (CMCC), and the Community Atmosphere Model Version 5.1 (CAM5) model. The models are forced by climatological SSTs [1981-2005 average from HadISST (Rayner et al. 2003)]. The GCM run by CMCC builds on ECHAM5 (Roeckner et al. 2003) with the same resolution employed in the CMCC fully coupled model (Scoccimarro et al. 2011): a T159 horizontal resolution, corresponding to a Gaussian grid of about 0.75° × 0.75° and a vertical resolution with 31 hybrid sigma-pressure levels with top at 10 hPa. The convection parameterization is based on the mass flux concept (Tiedtke 1989) modified following Nordeng (1994). Moist processes are treated using a mass conserving algorithm for the transport of the different water species and potential chemical tracers (Lin and Rood 1996). The transport is resolved on the Gaussian grid. A more detailed description of the ECHAM5 atmospheric model performance can be found in Roeckner et al. (2006).

134 The model used for this study is a newer version of the Geophysical Fluid Dynamics
135 Laboratory (GFDL) High Resolution Atmospheric Model (HIRAM) utilized in Zhao et al.
136 (2009), Zhao and Held (2010), and Held and Zhao (2011) for studies of global hurricane
137 climatology, variability, and change with global warming. It is a 50km resolution model using a
138 cubed-sphere dynamical core and the Bretherton et al. (2004) convection scheme for both
139 shallow and deep cumulus clouds. The main difference in the newer version is that it
140 incorporates a new land model (GFDL LM3). The atmospheric dynamical core of the model was
141 also updated to improve efficiency and stability. As a result of these changes, there are minor
142 retunings of the atmospheric parameters in the cloud and surface boundary layer
143 parameterizations necessary to achieve the top-of-atmosphere (TOA) radiative balance (Zhao et.
144 al 2012). This model is also the version of HIRAM used for the GFDL participation in the Fifth
145 Assessment Report of the Intergovernmental Panel on Climate Change (IPCC AR5) high-
146 resolution time-slice simulations.

147 The Community Atmospheric Model, version 5.1 (CAM5), developed by the U.S.
148 Department of Energy and the National Science Foundation was integrated using a finite volume
149 dynamical core on a latitude-longitude mesh of approximately 0.25^{o} with 30 vertical levels
150 (Bacmeister et al. 2013, Wehner et al. 2013). The CAM5 physical parameterization package uses
151 the Zhang and McFarlane (1995) deep convective parameterization and the University of
152 Washington (UW) shallow convection scheme (Park and Bretherton 2009). The convective
153 parameterization includes a dilute entraining plume (Neale et al. 2008) and a convective
154 momentum transport approximation as used in the previous version of the model, CAM4
155 (Richter and Rasch 2008). The moist boundary layer turbulence scheme is that of Bretherton and

156 Park (2009). A description of the surface flux parameterizations, an important driver for tropical
157 cyclogenesis, is described in Neale et al. (2010).

158 Each model had four simulations: (1) present day (Present-Day), (2) a doubling of CO_2 in the
159 atmosphere ($2\times CO_2$), (3) a uniform 2K rise in SST (+2K), and (4) a doubling of CO_2 plus a
160 uniform 2K rise in SST ($2\times CO_2$+2K). The number of years in terms of rainfall data varied from
161 model to model (20 years for GDFL, ten years for CMCC, and nine years for CAM5). The
162 tracking algorithm used to identify TCs in the GFDL outputs is similar to what is described in
163 Zhao et al. (2009). The tracking for the CMCC model is based on Walsh (1997) and Walsh et al.
164 (2007). Detailed information on the ability of climate models in representing TCs can be found
165 in Walsh et al. (2013). The tracking algorithm for the CAM5 model follows closely the method
166 and thresholds of Knutson et al (2007) and has been generalized to execute efficiently on very
167 large numbers of processors (Prabhat et al. 2011).

168 Here we focus on the evaluation of the highest rain-producing TCs both in the models and
169 observations. For each 1200 UTC time step of each TC in the IBTrACS or in the GFDL, CMCC
170 and CAM5 models, the rainfall in a 10°×10° grid around the center of circulation of the storm
171 was extracted based on the information available in the track files; these rainfall fields represent
172 daily rainfall accumulations and were then averaged over the storm lifetime to form a gridded
173 composite mean of the daily rainfall associated with a particular storm. We note that only time
174 steps when the TC center was south of 30°N (for the northern hemisphere), or north of 30°S (for
175 the southern hemisphere) were used to guard against extra-tropical dynamics affecting the TC
176 rainfall patterns. The composite mean TC rainfall patterns were then ranked according to the
177 highest average rainfall within a 5°-radius around the TC center, and the top 10% of the TCs
178 were selected. The selection of a 5°-radius around the TC center is consistent with other studies

179 in the literature (e.g., Hart and Evans 2001, Ren et al. 2006, Kunkel et al. 2010). We use a
180 percentage rather than a specific number of storms to account for differences in the number of
181 TCs in different basins and amongst the models. Finally all the TC time steps (or storm days) in
182 the top 10% of TCs were averaged to produce a composite mean of the TC storm days.
183 Supplementary Table 1 summarizes the number of TC storm days for each model, scenario and
184 basin. The western Pacific is the northern hemispheric basin with the largest number of TC days
185 with the exception of CAM5 (possibly due to a TC genesis more in the central Pacific, resulting
186 in storms counted in the eastern Pacific). We also notice the low TC activity in the CMCC model
187 in the north Atlantic and eastern Pacific due to this model's known issues in generating TCs in
188 these basins (Scoccimarro et al. 2011). The results presented in the next section are related to
189 TC-daily rainfall for the top 10% rainiest TCs.
190

191 ## 3. RESULTS

192 ### *3.1.Observations*

193 Figure 1 is based on GPCP data and shows the composite mean precipitation patterns
194 associated with the top-10% rainiest TCs in each of the six basins, together with the
195 corresponding hemispheric composites. For the northern hemisphere, the rainfall patterns have a
196 southwest-northeast orientation. The areas with maximum rainfall vary among the basins, from
197 the eastern quadrants in the north Atlantic to the southwest quadrant in the western Pacific; these
198 differences may partly be an artefact of the coarse resolution of GPCP (1°×1°), but are also likely
199 to be associated with the different storm morphology in these basins. There is also a large spread
200 in the number of TC storm days used in the composites, with the north Indian basin having the
201 fewest and the western Pacific the most fields used (see panel titles in Figure 1). The average

202 rainfall footprint is also very different from basin to basin. Most of the rainfall is concentrated
203 within a 5°-radius for the north Atlantic and the eastern Pacific, with the latter showing the
204 smallest rainfall averages among the basins in the northern hemisphere. On the other hand, the
205 rainfall footprint for the western Pacific is much larger, consistent with the discussion in Chan
206 and Chan (2012) related to the storm size in these basins. Overall, the TCs in the northern
207 hemisphere present a well-defined structure, with the largest composite daily rainfall close to the
208 center of circulation of the storms and decreasing as we move further away.

209 In the southern hemisphere the rainfall patterns tend to be mirror images of those observed in
210 the northern hemisphere, with a northwest-southeast structure, and the areas of maximum
211 composite rainfall predominantly occurring in the southeast TC quadrant. Beside the fact that
212 over the 1997–2012 period there were more than twice as many TC days in the northern
213 hemisphere compared with the southern hemisphere, another difference is related to the rainfall
214 magnitudes. In the southern hemisphere, while most of the (storm-relative) rainfall is within a
215 5°-radius of the storm center, on average the rainfall intensities are lower than in the northern
216 ocean basins. Part of the asymmetry in the rainfall patterns could be due to the storm motion and
217 the fact that we are working with rainfall at the daily scale.

218 The median radial profiles of composite TC rainfall rates have similar structure among the
219 different basins, with the highest rainfall rates near the center of circulation (Figure 2), and
220 differences that are related to the different interactions that these storms have with the
221 environment in which they develop in each basin (Lonfat et al. 2004). Owing to the coarse GPCP
222 resolution (1°×1°) the eyewall structure is not captured in these profiles. These profiles are
223 similar to the ones described in Jiang et al. (2008) for the north Atlantic, and Lonfat et al. (2004)
224 at the global scale once we account for GPCP's coarser resolution. More specifically, the TCs in

the northern Indian have the largest rainfall rates close to the center of circulation, and a rapid decrease as distance from the TC center increases. The storms in the western Pacific have the largest composite daily rainfall rates overall, in agreement with the results in Figure 1. Conversely, the eastern Pacific TCs are generally characterized by the smallest rainfall rates. Compared to the southern Indian, the average daily rainfall rates associated with storms in the southern Pacific is consistently larger for any distance from the storm center. The results for both hemispheres are consistent with the rainfall profiles in Lonfat et al. (2004).

3.2.Models

In this subsection we compare the rainfall patterns for the three models and examine the TC rainfall response to the three idealized warming scenarios. We will start with results at the global (Figure 3) and hemispheric scales (Supplementary Figures 1-2), and then examine changes in TC rainfall in each of the six ocean basins. At the global scale, the three models provide a consistent response to the different scenarios. In the $2\times CO_2$ run the intensity of the composite TC rainfall weakens compared to the Present-Day run. The reduction due to $2\times CO_2$ may be due to two superimposing components. The first is a reduction in global mean precipitation associated with a weaker radiative cooling rate due to a doubling in CO_2. The second is a weakening of TC intensity due to an increase in surface relative humidity and a slight increase of tropospheric stability (e.g., Sugi and Yoshimura 2004, Yoshimura and Sugi 2005, Held and Zhao 2011, Zhao et. al 2013). The +2K, and $2\times CO_2$ + 2K simulations both have higher rainfall than in the Present-Day one, which is due to the increased SST that leads to higher air temperatures, higher water vapour content and increased rainfall (Scoccimarro et al. 2013). Yoshimura and Sugi (2005) discuss the opposing effects of increasing SST and CO_2 in terms of precipitation and dry static stability. Our analyses lead to similar conclusions when we stratify the results into northern and

248 southern hemispheres (Supplementary Figures 1-2). Based on the summary values in Table 1 for
249 area- and daily-averaged precipitation associated with the top-10% rainiest TCs, our modelling
250 results indicate a reduction in precipitation in the doubling CO_2 scenario on the order of 5%
251 globally, and an increase in composite TC rainfall associated with a uniform increase of 2K in
252 SST (both alone and in combination with CO_2 doubling) on the order of 10-20% globally.

253 After performing analyses at the global and hemispheric scales, we focus on the each
254 individual ocean basin, comparing and contrasting the results from the three models under the
255 three warming scenarios at a much more regional scale. We start with the GFDL model. The
256 composite mean TC rainfall patterns for the four northern hemispheric basins for the Present-
257 Day and three warming simulations are shown in Figure 4. For the most part the patterns have an
258 ellipsoidal shape, with some structures exhibiting the expected southwest-northeast shape in the
259 northern hemisphere. Moreover, the rainfall patterns in the different basins tend to be similar to
260 the observations, with the TCs in the western (eastern) Pacific having the largest (smallest)
261 footprints. All basins, however, have maximum composite TC rainfall occurring in the top-left
262 quadrant, which differs from the observed patterns (Figure 1). Generally, the TC rainfall
263 intensities are comparable to the observations, with a tendency towards overestimation. To the
264 best of our knowledge, this is the first time that global comparisons between observed and
265 simulated TC rainfall composites have been performed.

266 Keeping in mind these similarities and differences between modelled and observed rainfall
267 while interpreting the following results, we now examine the potential changes in TC rainfall
268 under three different scenarios based on the GFDL model. In the $2\times CO_2$ run (Figure 4 second
269 column) the intensity of the composite TC rainfall weakens compared to the Present-Day
270 simulation (~5%-15%; Table 1), as shown by the reduced footprint of the largest rainfall areas.

In the case of $2\times CO_2$, atmospheric radiative cooling rate decreases due to a reduction of TOA (top of atmosphere) outgoing long-wave radiative flux. In equilibrium state, the reduction in atmospheric radiative cooling rate must balance by a reduction in surface precipitation and evaporation. Since surface winds do not change significantly in these GCMs, surface relative humidity must increase. The increase of surface relative humidity reduces surface evaporation potential (or thermodynamic disequilibrium), which is the primarily driving force for TC genesis and intensity. Thus, this explains the general reduction of TC rainfall intensity in the $2\times CO_2$ case. In addition, the increase in CO_2 concentration tend to slightly warm surface temperature over tropical lands which leads to slight warmer upper tropospheric temperature, contributing to a slight increase in tropospheric stability which may also be partially responsible for the reduction in rainfall intensity in the $2\times CO_2$ case. The +2K, and $2\times CO_2$ + 2K simulations both have higher TC rainfall rates than in the Present-Day run (up to 25% in the eastern Pacific; Table 1). These results are valid for all the northern hemispheric basins, with the exception of the north Atlantic, where TC rainfall intensity is higher than the Present-Day run for the +2K, but not for the $2\times CO_2$ + 2K (Table 1).

These results are corroborated in the median TC radial rainfall profiles in Figure 5 computed based on the top-10% rainiest TCs; the simulations for a 2K increase in global SST (whether with or without doubling CO_2) show the largest increase in rainfall at all distances. Similarly, a doubling of CO_2 alone results in a rainfall decrease at most ranges. These TC rainfall profiles also highlight the capability of the GFDL in capturing how the largest daily rainfall rates occur away from the storm center (approximately between 2° and 4°). These results are consistent with Lonfat et al. (2004) and Jiang et al. (2008), even though the maximum herein tends to occur further away than in the aforementioned observational studies.

294 In the south Indian and south Pacific basins, the maximum TC rainfall from the GFDL is
295 mostly in the bottom-left quadrant, the opposite of the northern hemisphere (cf. Figures 4 and 6).
296 There is some evidence for the southeast-northwest orientation in the composite mean rainfall
297 patterns, although the structures are not as well-defined as in the observations (Figure 1).
298 Moreover, there a tendency toward larger average TC rainfall values.

299 The rainfall response for the south Indian and south Pacific basins to different warming
300 scenarios in the GFDL is generally similar to the changes for the basins in the northern
301 hemisphere. The increase in global SST results in an overall increase in TC daily rainfall rates
302 (Table 1); on the other hand, a doubling of CO_2 results in comparable average rainfall values
303 (Table 1). The median rainfall profiles in Figure 5 (bottom panels) highlight the differences in
304 responses for the two basins. While for the southern Indian basin the median rainfall profiles
305 tend to be generally very similar regardless of the warming scenario, we observe more variability
306 in the southern Pacific. Interestingly, the TC rainfall in the +2K scenarios is generally the largest
307 close to the center of circulation, while it is the smallest for the $2\times CO_2$ one. On the other hand, as
308 we move away from the center of the storm, the largest rainfall intensities are for the $2\times CO_2$
309 scenario. These results suggest that, by doubling CO_2 we should expect a rainfall decrease close
310 to the center of the storm but also a widening of the areas associated with heavier rainfall.

311 We have also examined the potential changes in daily TC rainfall rates associated with a 2K
312 increase in SST based on the Clausius-Clapeyron relationship (14% increase in the Present-Day
313 scenario; Figure 5). For the north Atlantic, Knutson et al. (2013) found that the use of the
314 Clausius-Clapeyron relationship was able to well describe the TC rainfall rate changes at 200-
315 400km from the center of circulation, while other processes were dominant at shorter distances.
316 In our study and based on the GFDL global model, it is hard to find consistent results across

317 basins and range. In the north Atlantic and south Pacific Oceans, the TC rainfall changes in the
318 +2K scenario are in general agreement with what we would expect based on the Clausius-
319 Clapeyron relationship. On the other hand, with the exception of the eastern Pacific, the rainfall
320 increases in the other basins are less than what expected based on a 7%/K increase in
321 atmospheric humidity.

322 The regional rainfall composite and profile results for CMCC are similar to the ones
323 presented for the GFDL model for the six ocean basins and the three warming scenarios. Note
324 that the analyses related to the north Atlantic are presented but not discussed because of the
325 known issues that the CMCC model has in generating TCs in this basin (Scoccimarro et al.
326 2011). The same holds for the eastern Pacific, for which the number of TC days used to compute
327 the rainfall composites and profiles is much smaller than in the observations and in the GFDL
328 model. These deficiencies in sample size are too large to be ascribed to the shorter records
329 available for the CMCC model (10 years) and are more likely due to simulation deficiencies of
330 the model.

331 Figure 7 shows the composite TC daily rainfall patterns for the basins in the northern
332 hemisphere for the CMCC model. The rainfall composites for the storms in the western Pacific
333 and the north Indian oceans exhibit structures similar to those for the observations (Figure 1),
334 even though the TC rainfall amounts are generally larger. Moreover, the location of the areas
335 with the largest rainfall amounts is similar to those identified in the observations. The changes in
336 rainfall patterns for the different scenarios lead us to the same conclusions as those drawn for the
337 GFDL model.

338 By increasing the global SST by 2K, there is an increase in composite TC rainfall rates in the
339 western Pacific and the north Indian Oceans for the CMCC model. At the same time, rainfall

rates tend to decrease for the doubled CO_2 case (Table 1). This holds for both rainfall mean composites (Figure 7) and median radial profiles (Figure 8). Despite the coarser resolution of the CMCC model, there are still indications that the rainfall tends to increase from the center of the storm up to about 2°-3°, and decrease afterwards.

In the southern hemisphere the TC rainfall patterns from the CMCC model are similar to the observations (Figure 9). The major rainfall axis is oriented northwest to southeast as in Figure 1, even though the average rainfall tends to be higher than observed. The different warming scenarios provide results consistent with the northern hemisphere, as well as with those from the GFDL model. The global increase in SST results in an increase in TC rainfall rates, which is more marked closer to the center of the storms. On the other hand, in the $2\times CO_2$ scenario we observe a reduction in rainfall rates, with a narrowing of the areas of higher rainfall close to the center of circulation. These conclusions are also supported by the analyses of the rainfall profiles (Figure 8, bottom panels), in which warmer SST tends to translate to larger rainfall amounts, with some differences depending on the distance from the center (possibly related to the asymmetry of the precipitation near the center of the storms and changes in the location of maximum rainfall). If we try to interpret the changes in rainfall profile using the Clausius-Clapeyron relationship, we have results similar to those for the GFDL model, with the profiles for the +2K scenario exhibiting less rainfall than expected according to a 7%/K increase in atmospheric moisture. There is actually a better agreement between the $2K+2\times CO_2$ profiles and those based on a 14% increase in rainfall from the Present-Day scenario.

The CAM5 is the model with the highest spatial resolution (approximately 0.25°). There are both similarities and differences with respect to the observational record and the other two models at the ocean-basin scale. Qualitatively, the TC rainfall patterns for the Present-Day runs

are consistent with the observations and the other models, even though the rainfall values tend to be larger than those based on GPCP and the fields are less smooth because of the higher spatial resolution (Figure 10). There are a few differences in terms of the TC rainfall days. In the observations and the GFDL and CMCC models, the western Pacific has the largest number of TC days, followed by the eastern Pacific. For the CAM5 model, on the other hand, the number of TC storm days is the largest for the eastern Pacific, followed by the western Pacific. Despite the differences in TC days, the storms in the western Pacific are the ones with the largest composite rainfall footprint followed by the north Atlantic TCs. Finally, while the CMCC and GFDL models and observations indicate that the rainfall associated with eastern Pacific TCs is the smallest among the basins in the northern hemisphere, this is not the case for the CAM5 model, for which storms in the north Indian Ocean have the smallest rainfall values.

Examination of the model results for the three warming scenarios for the CAM5 model does not allow a consistent interpretation of the results for all the basins. Compared to the Present-Day climate runs (Table 1), the rainfall associated with north Atlantic, western Pacific and north Indian TCs decreases for a doubling in CO_2, while it increases for the eastern Pacific storms. On the other hand, there is a general increase in TC rainfall rates for the two scenarios involving a +2K increase in global SST (Table 1). The differences among scenarios can also be assessed for different distances from the center of circulation (Figure 11, top and middle rows). Despite the finer resolution, there is not the clear enhancement in rainfall rates as we move 100-300km from the center of circulation discussed for the GFDL model and reported in observational studies (e.g., Lonfat et al. 2004, Jiang et al. 2008). We can also clearly see the changes in rainfall profiles in response to the different scenarios. Based on the GFDL and the CMCC models and published studies (e.g., Sugi and Yoshimura 2004, Yoshimura and Sugi 2005), we would have

386 expected a decrease in rainfall associated with a CO_2-doubling. The response to increasing global
387 SST is generally consistent with the other models.

388 Figure 12 shows the composite mean daily TC rainfall rate patterns for the basins in the
389 southern hemisphere for the CAM5 model. The results for the Present-Day climate are similar to
390 the observational record, with the same orientation and larger rainfall associated with the storms
391 in the south Pacific rather than in the south Indian Ocean. For both basins, there is an overall
392 decrease in TC rainfall rates for the $2\times CO_2$ scenario (Table 1). In the +2K case, there is an
393 increase in TC rainfall for the south Indian and a marginal decrease for the south Pacific. Finally,
394 more TC rainfall is generally associated with the $2\times CO_2$+2K scenario.

395 The TC rainfall profiles based on the CAM5 model for the two basins in the southern
396 hemisphere show similarities and differences with respect to the other models. For the south
397 Indian, there is not a large degree of variability among scenarios (see Figures 5 and 8 for
398 comparison with the GFDL and CMCC models). On the other hand, the median profiles for the
399 TCs in the south Pacific suggest an overall reduction in TC rainfall in the three warming
400 scenarios compared to the Present-Day run, in particular close to the center of circulation. This
401 response is different from what is observed in the other models regardless of the ocean basin.
402 Further work is necessary to assess what the possible causes for the discrepancies between
403 CAM5 and the GFDL and CMCC are in the south Pacific. Similar to what was found for the
404 CMCC and GFDL models, it is difficult to interpret the results associated with the +2K scenario
405 in terms of a simple Clausius-Clapeyron relationship scaling argument.

406 ## 4. CONCLUSIONS

407 This study aimed to examine potential changes in rainfall associated with TCs at the global
408 scale under different idealized global-scale perturbations. Results are based on three state-of-the-

art atmospheric models (GFDL, CMCC and CAM5) and three idealized perturbation atmospheric general circulation experiments (the radiative perturbation from doubling CO_2 but keeping SST fixed, increasing the global SST by 2K, and a combination of the two).

An important step we undertook prior to the examination of the models' response to the different scenarios involved the assessment of the models' capability in reproducing the TC rainfall patterns in the observational records. Our findings suggest that these models are able to characterize the rainfall rate distribution associated with TCs reasonably well, both in terms of rainfall mean spatial composites and radial profiles. Our results, however, also indicate that there are discrepancies between modelled and observed TC rainfall. These discrepancies are related to both the location of the rainfall maximum and the rainfall magnitudes. Despite the relevance of the TC rainfall hazard, it appears that the model evaluation of the rainfall fields is generally lacking in a number of studies describing modelling of TC activity. We hope that this study could represent a first step towards a more comprehensive and widespread effort in assessing the skill of models in reproducing the rainfall properties associated with TCs.

With these model limitations in mind, we examined how TC rainfall would change in response to three forcing perturbations. Even though we highlighted some differences among models and basins, our results point to a reduction in composite TC rainfall rates (both in terms of spatial extent and magnitude) in direct response to a doubling in CO_2, with SSTs remaining unchanged. On the other hand, a 2K global increase in SST points to the opposite result, with an overall increase in TC rainfall rates in all models. The spatial structure of the precipitation changes are less consistent than the spatially-averaged changes, and we found that there are no consistent patterns among basins and distance from the center of circulation. Results at the global and hemispheric scales point to an average TC rainfall reduction when doubling CO_2 on the

order of 5%, and an increase associated with a global warming of the SST by 2K (both alone and in combination with CO_2 doubling) on the order of 10-20%. For individual basins, the response seen in the global and hemispheric means is recovered, although with slightly more inter-model spread, and some inter-basin differences. However, the overall tendency of the rainfall in the idealized perturbations is recovered across most basins for all models (Table 1), including the increase in response to a combined doubling of CO_2 and an increase in global SST. There are indications that the response to both doubling of CO_2 and 2K warming together is not a linear sum of the responses to each forcing agent individually (Table 1), with the area-averaged increase in TC rainfall in response to both forcing agents often exceeding the increase in response to a 2K increase alone – even though the response to CO_2 increases alone is for a precipitation decrease. Because this result was unexpected to us, and because of the relatively small sample size, we choose to stop at remarking on its apparent existence, but leave further exploration and assessment of its mechanisms – to the extent that it is real – to future work.

These results add to an expectation that greenhouse gas induced tropical warming should lead to an increase in rainfall rates of individual TCs (e.g., Knutson and Tuleya 2004; Knutson et al. 2010, 2013). Current generation GCMs project, under a wide range of projected 21st century forcing scenarios, a robust warming of the tropics and tropical cyclone basins over the 21st century (e.g., Zhao et al. 2009, Vecchi and Soden 2007, Villarini and Vecchi 2012, Knutson et al. 2013). Based on these projections, an increase in SST by 2K over their study area is within the realm of possibilities – arising largely from, and accompanied by, increases in greenhouse gases. Our results indicate that the decreases in TC precipitation rates from CO_2 increases alone are not sufficient, in these three GCMs, to compensate for the SST-driven increases in TC rainfall rates. If current GCM projections of tropical warming and the rainfall modelling results

455 described here and elsewhere are realized, then the hazard associated with rainfall from
456 individual TCs should be increasing over the course of this century.
457
458
459 *Acknowledgements*
460 This work was carried out as part of a Hurricane and Climate Working Group activity supported
461 by the U.S. CLIVAR. We acknowledge the support provided by Naomi Henderson, who
462 downloaded and organized the data at the Lamont data library. Gabriele Villarini and David
463 Lavers acknowledge financial support from the Iowa Flood Center, IIHR-Hydroscience &
464 Engineering. This material is based in part upon work supported by the National Science
465 Foundation under Grant No. AGS-1262099 (Gabriele Villarini and Gabriel A. Vecchi), and in
466 part from the Italian Ministry of Education, University and Research and the Italian Ministry of
467 Environment, Land and Sea under the GEMINA project (Enrico Scoccimarro). Michael Wehner
468 was supported by the Regional and Global Climate Modeling Program of the Office of
469 Biological and Environmental Research in the Department of Energy Office of Science under
470 contract number DE-AC02-05CH11231. CAM5 calculations were performed at the National
471 Energy Research Supercomputing Center (NERSC) at the Lawrence Berkeley National
472 Laboratory.
473

REFERENCES

Bacmeister, J.T., R.B. Neale, C. Hannay, J. Truesdale, J. Caron, P. Lauritzen, A. Gettelman, and M. Wehner, 2013: High-resolution climate simulations using the Community Atmosphere Model (CAM). *J. Climate* (in press).

Bretherton, C.S., and S. Park, 2009: A new moist turbulence parameterization in the Community Atmosphere, Model. *J. Climate*, 22, 3422–3448.

Bretherton, C.S., J.R. McCaa, and H. Grenier, 2004: A new parameterization for shallow cumulus convection and its application to marine subtropical cloud-topped boundary layers. Part I: Description and 1D results. *Mon. Wea. Rev.*, **132**, 864–882.

Camargo, S.J., A.G. Barnston, and S.E. Zebiak, 2005: A statistical assessment of tropical cyclone activity in atmospheric general circulation models. *Tellus*, 57A: 589-604.

Chan, K.T.F., and J.C.L. Chan, 2012: Size and strength of tropical cyclones as inferred from QuickSCAT Data. *Mon. Wea. Rev.*, **140**, 811-824.

Czajkowski, J., K. Simmons, and D. Sutter, 2011: An analysis of coastal and inland fatalities in landfalling US hurricanes. *Nat. Hazards*, **59**, 1513-1531.

Czajkowski, J., G. Villarini, E. Michel-Kerjan, and J.A. Smith, 2013: Determining tropical cyclone inland flooding loss on a large-scale through a new flood peak ratio-based methodology. Submitted to *Environ. Res. Lett.*

Emmanuel, K. 2005: Increasing destructiveness of tropical cyclones over the past 30 years. *Nature*, **436**, 686-688.

Hart, R.E., and J.L. Evans, 2001: A climatology of the extratropical transition of Atlantic tropical cyclones. *J. Climate*, 14, 546-564.

Held, I.M. and M. Zhao, 2011: The response of tropical cyclone statistics to an increase in CO_2 with fixed sea surface temperatures. *J. Climate*, **24,** 5353-5364.

Huffman, G.J., R.F. Adler, M. Morrissey, D.T. Bolvin, S. Curtis, R. Joyce, B. McGavock, and J. Susskind, 2001: Global precipitation at onedegree daily resolution from multi-satellite observation. *J. Hydrometeorol*., **2**, 36–50.

Jiang, H., J.B. Halverson, J. Simpson, and E.J. Zipser, 2008: Hurricane "rainfall potential" derived from satellite observations aids overland rainfall prediction. *J. Appl. Meteorol. Clim.*, **47**, 944-959.

Jonkman, S.N., B. Maaskant, E. Boyd, and M. L. Levitan, 2009: Loss of life caused by the flooding of New Orleans after Hurricane Katrina: Analysis of the relationship between flood characteristics and mortality. *Risk Anal.*, **29**(5), 676-698.

Knapp, K.R., M.C. Kruk, D.H. Levinson, H.J. Diamond, and C.J. Neumann, 2010: The International Best Track Archive for Climate Stewardship (IBTrACS): Unifying tropical cyclone best track data. *Bull. Amer. Meteor. Soc*., **91**, 363-376.

Knutson, T.R., and R.E. Tuleya, 2004: Impact of CO_2-induced warming on simulated hurricane intensity and precipitation: Sensitivity to the choice of climate model and convective parameterization. *J. Climate,* **17,** 3477–3495.

Knutson, T. R., and Coauthors, 2010: Tropical cyclones and climate change. *Nat. Geosci.*, **3**, 157–163.

Knutson, T.R., J.J. Sirutis, S.T. Garner, I.M. Held, R.E. Tuleya, 2007: Simulation of the recent multidecadal increase of Atlantic hurricane activity using an 18-km-grid regional model. *Bull. Amer. Meteor. Soc.*, **88**, 1549–1565.

518 Knutson, T.R., J.J. Sirutis, G.A. Vecchi, S. Garner, M. Zhao, H.-S. Kim, M. Bender, R.E.
519 Tuleya, I.M. Held, and G. Villarini, 2013: Dynamical downscaling projections of twenty-
520 first-century Atlantic hurricane activity: CMIP3 and CMIP5 model-based scenarios. *J.*
521 *Climate*, **26**(17), 6591-6617.
522 Kunkel, K.E., D. Easterling, D.A.R. Kristovich, B. Gleason, L. Stoecker, and R. Smith, 2010:
523 Recent increases in U.S. heavy precipitation associated with tropical cyclones. *Geophys.*
524 *Res. Lett.*, **37**, L24706, doi:10.1029/2010GL045164.
525 Lau, W.K.M., and Y.P. Zhou, 2012: Observed recent trends in tropical cyclone rainfall over the
526 North Atlantic and the North Pacific. *J. Geophys. Res.*, **117**, D03104,
527 doi:10.1029/2011JD016510.
528 Lin, S.J., and R.B. Rood, 1996: Multidimensional flux form semi-Lagrangian transport. *Mon.*
529 *Wea. Rev.*, 124, 2046–2068.
530 Lonfat, M., F.D. Marks, and S.S. Chen, 2004: Precipitation distribution in tropical cyclones
531 using the Tropical Rainfall Measuring Mission (TRMM) Microwave Imager: A global
532 perspective. *Mon. Wea. Rev.*, **132**, 1645-1660.
533 Mendelsohn, R., K. Emanuel, S. Chonabayashi, and L. Bakkensen, 2012: The impact of climate
534 change on global tropical cyclone damage. *Nat. Clim. Change*, **2**, 205-209.
535 Neale, R.B., C.-C. Chen, A. Gettelman P.H. Lauritzen, S. Park, D.L. Williamson, A.J. Conley, R.
536 Garcia, D. Kinnison, J.-F. Lamarque, D. Marsh, M. Mills, A.K. Smith, S. Tilmes, F. Vitt,
537 H. Morrison, P. Cameron-Smith, W.D. Collins, M.J. Iacono, R.C. Easter, S.J. Ghan, X.
538 Liu, P.J. Rasch, and M.A. Taylor, 2010: Description of the NCAR Community
539 Atmosphere Model (CAM 5.0). NCAR Tech. Note NCAR/TN-486+STR, National
540 Center for Atmospheric Research, Boulder, Colorado. 282 pp.
541 Nordeng, T.E., 1994: Extended versions of the convective parametrization scheme at ECMWF
542 and their impact on the mean and transient activity of the model in the tropics. ECMWF
543 Research Department Tech. Memo. 206, 41 pp.
544 Peduzzi, P., B. Chatenou, H. Dao, A. De Bono, C. Herold, J. Kossin, F. Mouton, and O.
545 Nordbeck, 2012: Global trends in tropical cyclone risk. *Nat. Climate Change*, **2**, 289–
546 294.
547 Park, S., and C.S. Bretherton, 2009: The University of Washington shallow convection and moist
548 turbulence schemes and their impact on climate simulations with the Community
549 Atmosphere Model. *J. Climate*, 22, 3449–3469.
550 Pielke, R.A., J. Gratz, C.W. Landsea, D. Collins, M.A. Saunders, and R. Musulin, 2008:
551 Normalized hurricane damage in the United States: 1900-2005. *Nat. Hazards Rev.*, **9**(1),
552 29–42.
553 Prabhat, O. Ruebel, S. Byna, K. Wu, F. Li, M.Wehner, and W. Bethel, 2012: TECA: A Parallel
554 Toolkit for Extreme Climate Analysis, International Conference on Computational
555 Science, ICCS 2012, Workshop on Data Mining in Earth System Science, *Proc. Comp.*
556 *Sci.*
557 Rappaport, E.N., 2000: Loss of life in the United States associated with recent tropical cyclones.
558 *Bull. Amer. Meteor. Soc.*, **81,** 2065–2074.
559 Rayner, N.A., D.E. Parker, E.B. Horton, C.K. Folland, L.V. Alexander, D.P. Rowell, E.C. Kent,
560 and A. Kaplan, 2003: Global analyses of sea surface temperature, sea ice, and night
561 marine air temperature since the late nineteenth century. *J. Geophys. Res.*, **108** (D14),
562 doi:10.1029/2002JD002670.

563 Ren, F., G. Wu, W. Dong, X. Wang, Y. Wang, W. Ai, and W. Li, 2006: Changes in tropical
564 cyclone precipitation over China. *Geophys. Res. Lett.*, **33**, doi:10.1029/2006GL027951.
565 Richter, J.H., and P.J. Rasch, 2008: Effects of convective momentum transport on the
566 atmospheric circulation in the Community Atmosphere Model, version 3. *J. Climate*, 21,
567 1487–1499.
568 Roeckner, E., and Coauthors, 2003: The atmospheric general circulation model ECHAM5. Part
569 I: Model description. MPI Rep. 349, 127 pp.
570 Roeckner E. and Coauthors, 2006: Sensitivity of simulated climate to horizontal and vertical
571 resolution in the ECHAM5 atmosphere model. *J. Climate*, **19**, 3771–3791.
572 Scoccimarro, E., S. Gualdi, A. Bellucci, A. Sanna, P.G. Fogli, E. Manzini, M. Vichi, P. Oddo,
573 and A. Navarra, 2011: Effects of tropical cyclones on ocean heat transport in a high-
574 resolution coupled general circulation model. *J. Climate*, **24**, 4368-4384.
575 Scoccimarro, E., S. Gualdi, G. Villarini, G. Vecchi, M. Zhao, K. Walsh and A. Navarra, 2013:
576 Intense precipitation events associated with landfalling tropical cyclones in a warmer
577 climate. Submitted to *J. Climate*.
578 Sugi, M., and J. Yoshimura, 2004: A mechanism of tropical precipitation change due to CO_2
579 increase. *J. Climate*, **17**, 238-243.
580 Taylor, K.E., R.J. Stouffer, and G.A. Meehl, 2012: An overview of CMIP5 and the experiment
581 design. *Bull. Amer. Meteor. Soc.*, **93**, 485–498.
582 Tiedtke, M., 1989: A comprehensive mass flux scheme for cumulus parametrization in large-
583 scale models. *Mon. Wea. Rev.*, **117**, 1779–1800.
584 Vecchi, G.A., and B.J. Soden, 2007: Effect of remote sea surface temperature change on tropical
585 cyclone potential intensity, *Nature*, 450, 1066-1070 doi:10.1038/nature06423.
586 Villarini, G., and G.A. Vecchi, 2012: Twenty-first-century projections of North Atlantic tropical
587 storms from CMIP5 models. *Nat. Climate Change*, **2**, 604-607.
588 Walsh, K.J.E., 1997: Objective detection of tropical cyclones in high-resolution analyses. *Mon.*
589 *Wea. Rev.*, **125**, 958–977.
590 Walsh, K.J.E., M. Fiorino, C.W. Landsea, and K.L. McInnes, 2007: Objectively determined
591 resolution-dependent threshold criteria for the detection of tropical cyclones in climate
592 models and reanalyses. *J. Climate*, **20**, 2307–2314.
593 Walsh, K.J.E., S. Lavender, E. Scoccimarro and H. Murakami, 2013: Resolution dependence of
594 tropical cyclone formation in CMIP3 and finer resolution models. *Clim. Dynam.*, **40**,
595 585–599, doi: 10.1007/s00382-012-1298-z.
596 Wehner, M.F., K.A. Reed, F. Li, Prabhat, J. Bacmeister, C.-T. Chen, C. Paciorek, P. Gleckler, K.
597 Sperber, W.D.Collins, A. Gettelman, C. Jablonowski, and C. Algieri, 2013: The effect of
598 horizontal resolution on simulation quality in the Community Atmospheric Model,
599 CAM5.1. Submitted to the *J. Modeling Earth Sys*.
600 Ying, M., B. Chen, and G. Wu, 2011: Climate trends in tropical cyclone-induced wind and
601 precipitation over mainland China. *Geophys. Res. Lett.*, **38**, doi:10.1029/2010GL045729.
602 Yoshimura, J., and M. Sugi, 2005: Tropical cyclone climatology in a high-resolution AGCM –
603 Impacts of SST warming and CO_2 increase. *SOLA*, **1**, 133-136.
604 Zhang, G.J., and N.A. McFarlane, 1995: Sensitivity of climate simulations to the
605 parameterization of cumulus convection in the Canadian Climate Centre General
606 Circulation Model. *Atmos.– Ocean*, 33, 407–446.
607 Zhang, Q., L. Wu, and Q. Liu, 2009: Tropical cyclone damages in China 1983–2006. *Bull. Amer.*
608 *Meteor. Soc.*, **90**, 489–495.

609 Zhao, M., and I. M. Held, 2010: An analysis of the effect of global warming on the intensity of
610 Atlantic hurricanes using a GCM with statistical refinement. *J. Climate*, **23**, 6382–6393.
611 Zhao, M., and I. M. Held, 2012: TC-permitting GCM simulations of hurricane frequency
612 response to sea surface temperature anomalies projected for the late-twenty-first century.
613 *J. Climate*, **25**, 2995–3009.
614 Zhao, M., I.M. Held, S.-J. Lin, and G.A. Vecchi, 2009: Simulations of global hurricane
615 climatology, interannual variability, and response to global warming using a 50-km
616 resolution GCM. *J. Climate*, **22**, 6653–6678.
617 Zhao, M., I. M. Held, and S.-J. Lin, 2012: Some counter-intuitive dependencies of tropical
618 cyclone frequency on parameters in a GCM. *J. Atmos. Sci.*, **69**, 2272-2283.
619 Zhao, M., I. M. Held, G. A. Vecchi, and Coauthors, 2013: Robust direct effect of increasing
620 atmospheric CO_2 concentration on global tropical cyclone frequency: a multi-model
621 inter-comparison. *U.S. CLIVAR Variations*, **11**(3), 17-23.
622

LIST OF TABLES

LIST OF FIGURES

Figure 1: Composite mean observed (GPCP) daily rainfall rate patterns in the six ocean basins, as well as the composites for the northern and southern hemispheres' top-10% rainiest TCs. The number of TC storm days used in the composite is given in the panel titles. The units are mm/day, and the x and y axes correspond to degrees from the TC center.

Figure 2: Top panel: Median radial rainfall profiles for the northern hemispheric basins including the north Atlantic (NA), eastern Pacific (EP), western Pacific (WP), north Indian (NI), and all northern hemispheric basins (NH). Bottom panel: Median radial rainfall profiles for the southern hemispheric basins including the south Indian (NI), south Pacific (SP), and all southern hemispheric basins (SH). The units are mm/day, and the x axis corresponds to degrees from the TC center.

Figure 3: Composite weighted mean daily rainfall rate patterns at the global scale for each of the three models and the different scenarios. The weights are computed based on the number of TC storm days in each basin (see Supplementary Table 1). The units are mm/day, and the x and y axes correspond to degrees from the TC center. Note that the color bar extends over a different range for the GFDL model.

Figure 4: Composite mean daily rainfall patterns (in mm/day) for the storm days in the top-10% rainiest TCs in the four GFDL simulations (columns) and in the four northern hemispheric TC basins (rows). The number of TC storm days used in each composite is given in the panel titles, and the x and y axes correspond to degrees from the TC center of circulation.

Figure 5: Median radial rainfall profiles for the northern (top two rows) and southern (bottom panels) hemispheric basins in the four GFDL simulations. (X axis corresponds to degrees from the TC center. The line "Present Day (CC)" refers to the rainfall profile for the "Present Day" increased by 14%, corresponding to a moisture increase according to the Clausius-Clapeyron relationship for a 2K increase in SST. The bin size is 1 decimal degree.

Figure 6: Composite mean daily rainfall patterns (in mm/day) for the storm days in the top-10% rainiest TCs in the four GFDL simulations (rows) and in the two southern hemispheric TC basins (columns). The number of TC storm days used in each composite is given in the panel titles, and the x and y axes correspond to degrees from the TC center.

Figure 7: As in Figure 4, but for the CMCC model. Note that the color bar extends over twice the range in Figure 4.

Figure 8: As in Figure 5, but for the CMCC model.

Figure 9: As in Figure 6, but for the CMCC model.

Figure 10: As in Figure 4, but for the CAM5 model. Note that the color bar extends over twice the range in Figure 4.

675 Figure 11: As in Figure 5, but for the CAM5 model. Note that 0.5° bins are used instead of the 1°
676 bins used in Figures 5 and 8.
677
678 Figure 12: As in Figure 6, but for the CAM5 model.
679

680 Table 1. Percentage changes of the three warming scenarios with respect for the Present-Day
681 runs for the three models for the different basins and at the global and hemispheric scales.
682 Results are representative of a 5°-radius area around the center of circulation for each storm.

683

	GFDL			CMCC			CAM5		
	$2\times CO_2$	+2K	$2\times CO_2$+2K	$2\times CO_2$	+2K	$2\times CO_2$+2K	$2\times CO_2$	+2K	$2\times CO_2$+2K
Global	-6.1	9.1	11.7	-5.4	10.7	12.8	-1.4	13.2	16.5
North hemisphere	-8.9	7.8	13.3	-6.7	15.7	17.1	1.3	14.1	16.1
South hemisphere	0.4	12.6	8.8	-6.2	0.9	4.5	-8.0	10.1	18.0
North Atlantic	-16.7	18.2	-11.8	-1.8	4.5	11.1	-8.4	-0.4	8.5
East Pacific	-6.5	25.1	17.0	-6.0	14.0	24.3	12.9	17.0	27.8
West Pacific	-5.9	2.5	16.5	-8.1	15.8	14.8	-11.1	17.1	3.7
North Indian	-17.7	0.2	17.6	1.7	21.0	21.2	-1.5	18.7	19.2
South Indian	1.1	7.3	5.8	-9.5	-1.8	-1.4	-7.6	16.4	25.6
South Pacific	-0.9	19.9	12.9	-4.5	1.8	5.3	-10.3	-0.3	10.6

684

685

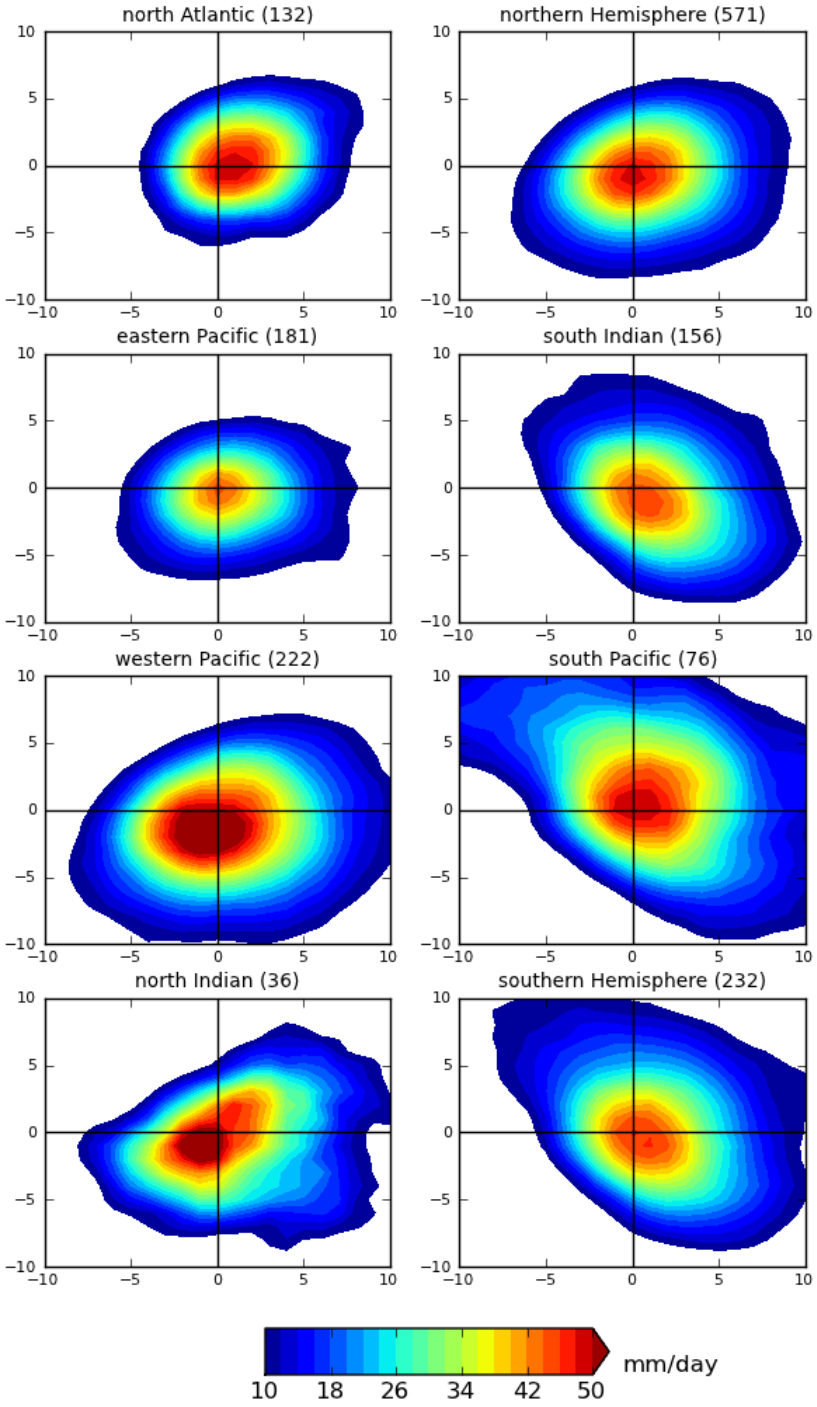

686

687 Figure 1: Composite mean observed (GPCP) daily rainfall rate patterns in the six ocean basins,
688 as well as the composites for the northern and southern hemispheres' top-10% rainiest TCs. The
689 number of TC storm days used in the composite is given in the panel titles. The units are
690 mm/day, and the x and y axes correspond to degrees from the TC center.

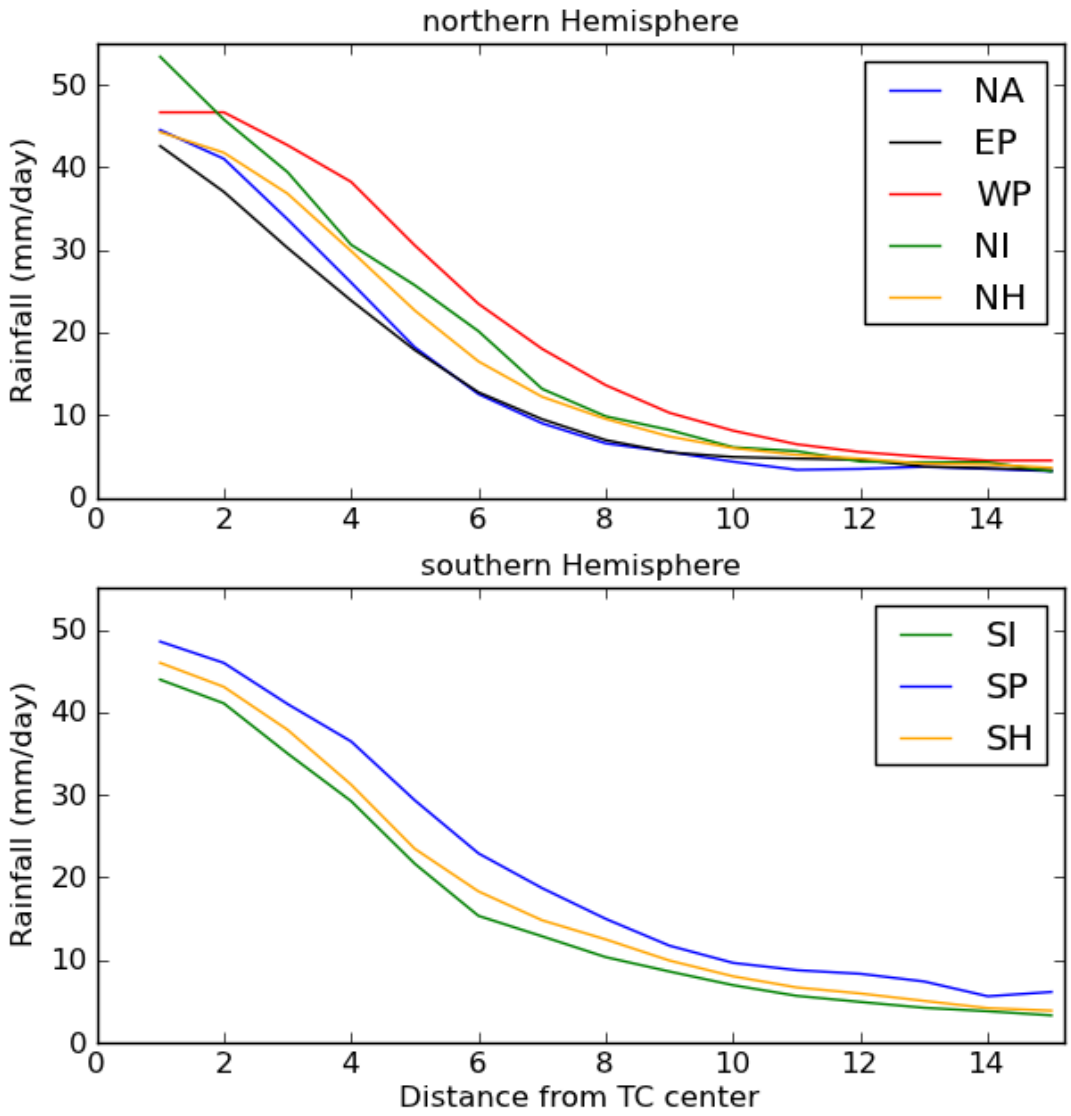

691

692 Figure 2: Top panel: Median radial rainfall profiles for the northern hemispheric basins including
693 the north Atlantic (NA), eastern Pacific (EP), western Pacific (WP), north Indian (NI), and all
694 northern hemispheric basins (NH). Bottom panel: Median radial rainfall profiles for the southern
695 hemispheric basins including the south Indian (NI), south Pacific (SP), and all southern
696 hemispheric basins (SH). The units are mm/day, and the x axis corresponds to degrees from the
697 TC center.

698

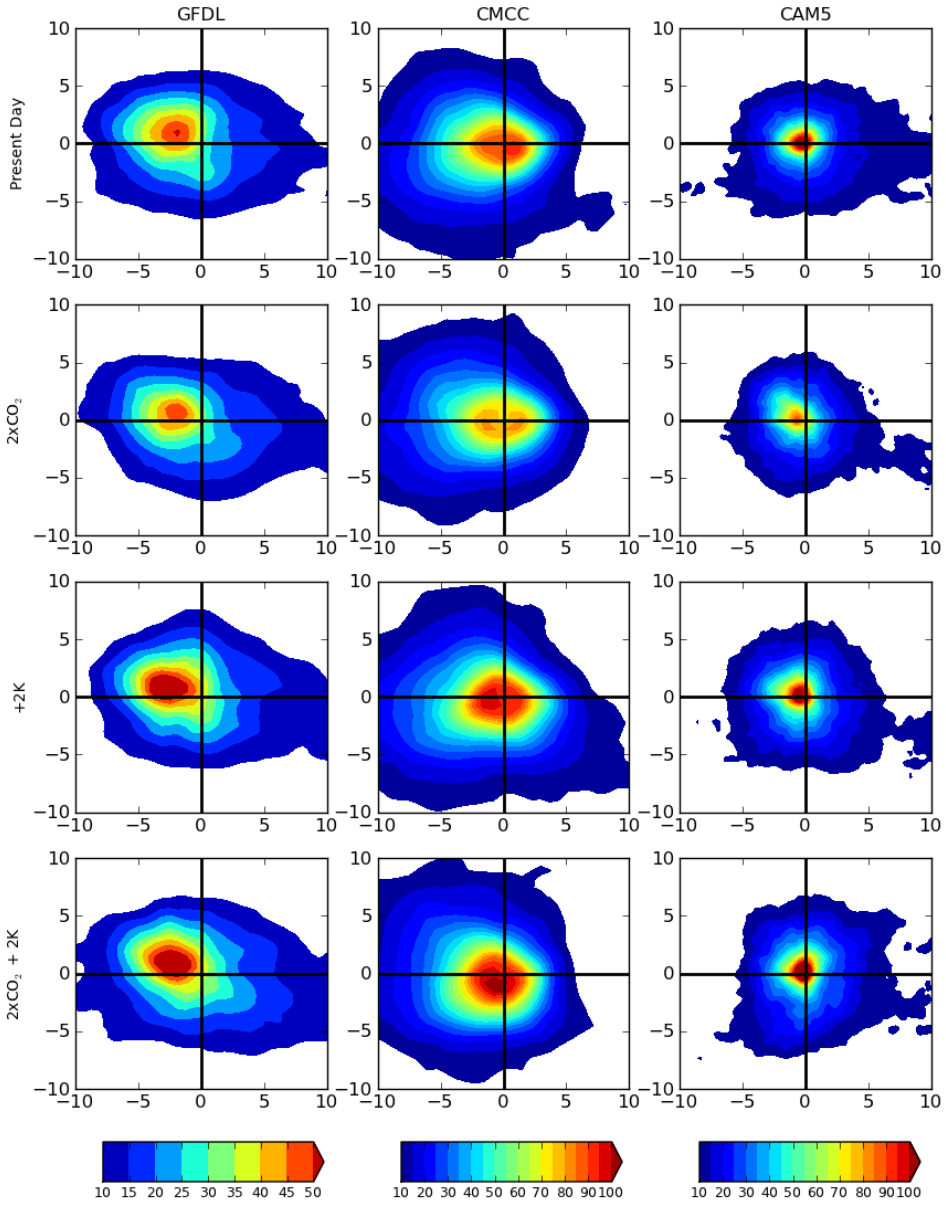

Figure 3: Composite weighted mean daily rainfall rate patterns at the global scale for each of the three models and the different scenarios. The weights are computed based on the number of TC storm days in each basin (see Supplementary Table 1). The units are mm/day, and the x and y axes correspond to degrees from the TC center. Note that the color bar extends over a different range for the GFDL model.

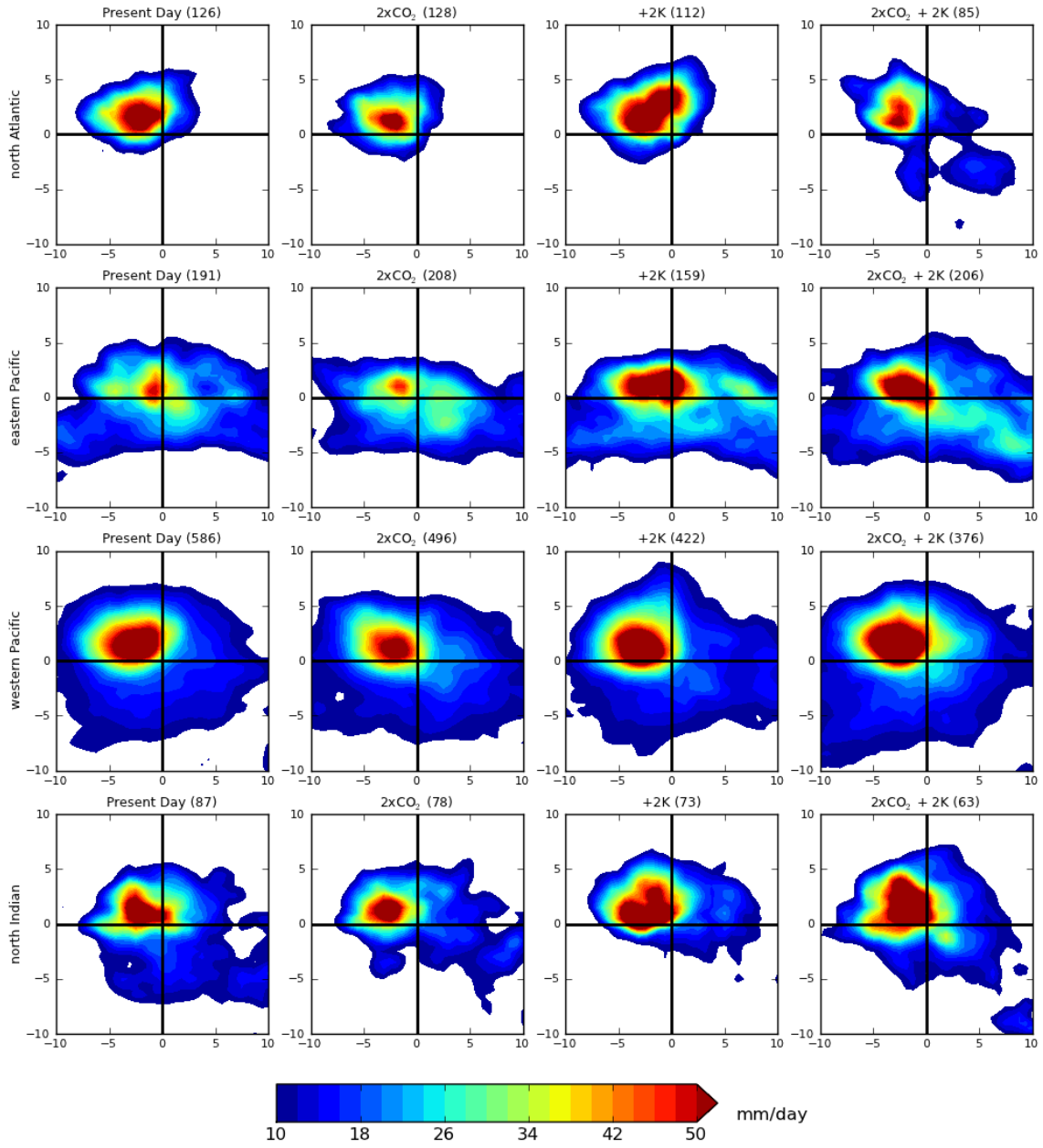

707

708 Figure 4: Composite mean daily rainfall patterns (in mm/day) for the storm days in the top-10%
709 rainiest TCs in the four GFDL simulations (columns) and in the four northern hemispheric TC
710 basins (rows). The number of TC storm days used in each composite is given in the panel titles,
711 and the x and y axes correspond to degrees from the TC center of circulation.

712

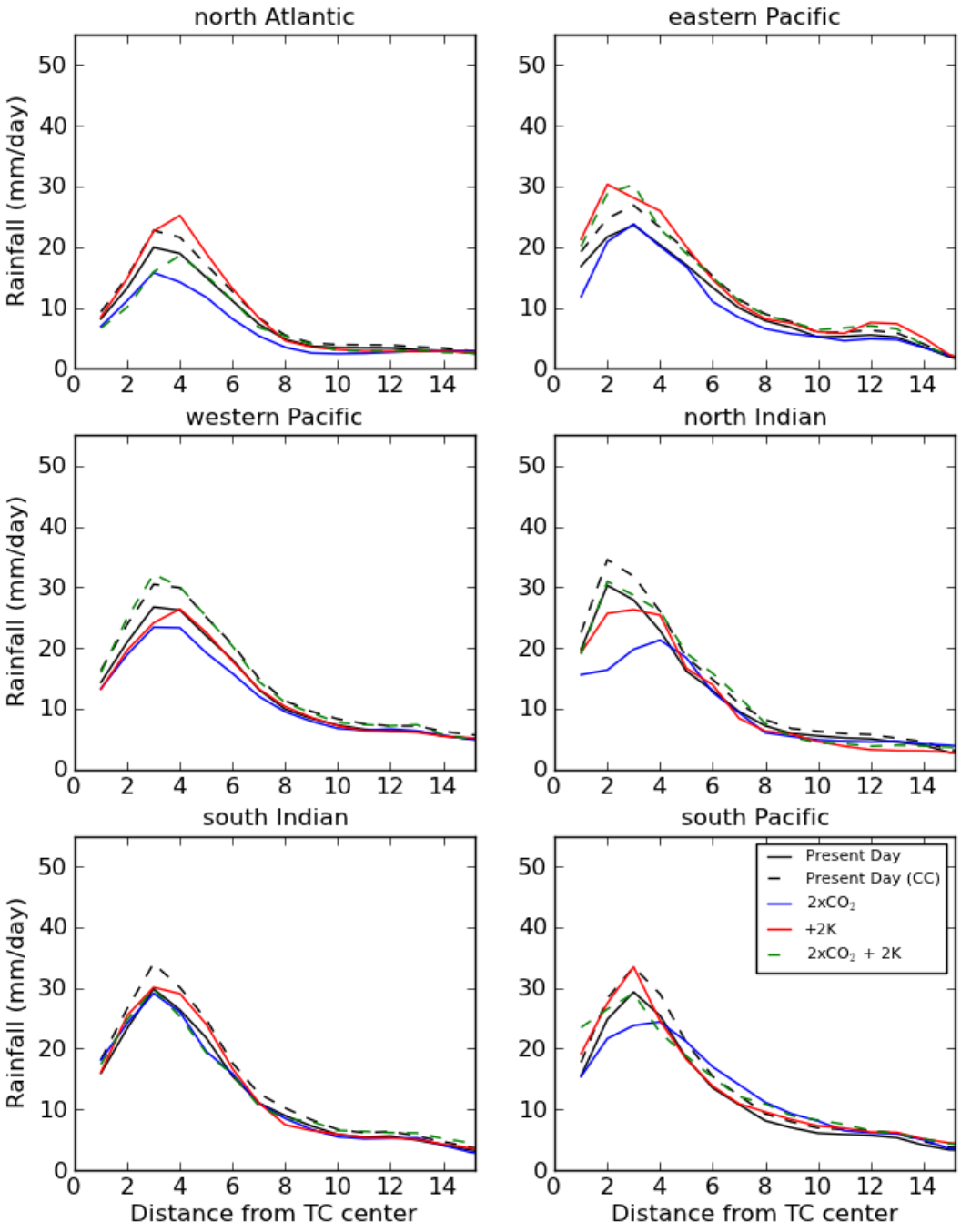

713

714 Figure 5: Median radial rainfall profiles for the northern (top two rows) and southern (bottom

715 panels) hemispheric basins in the four GFDL simulations. (X axis corresponds to degrees from

716 the TC center. The line “Present Day (CC)” refers to the rainfall profile for the “Present Day”
717 increased by 14%, corresponding to a moisture increase according to the Clausius-Clapeyron
718 relationship for a 2K increase in SST. The bin size is 1 decimal degree.

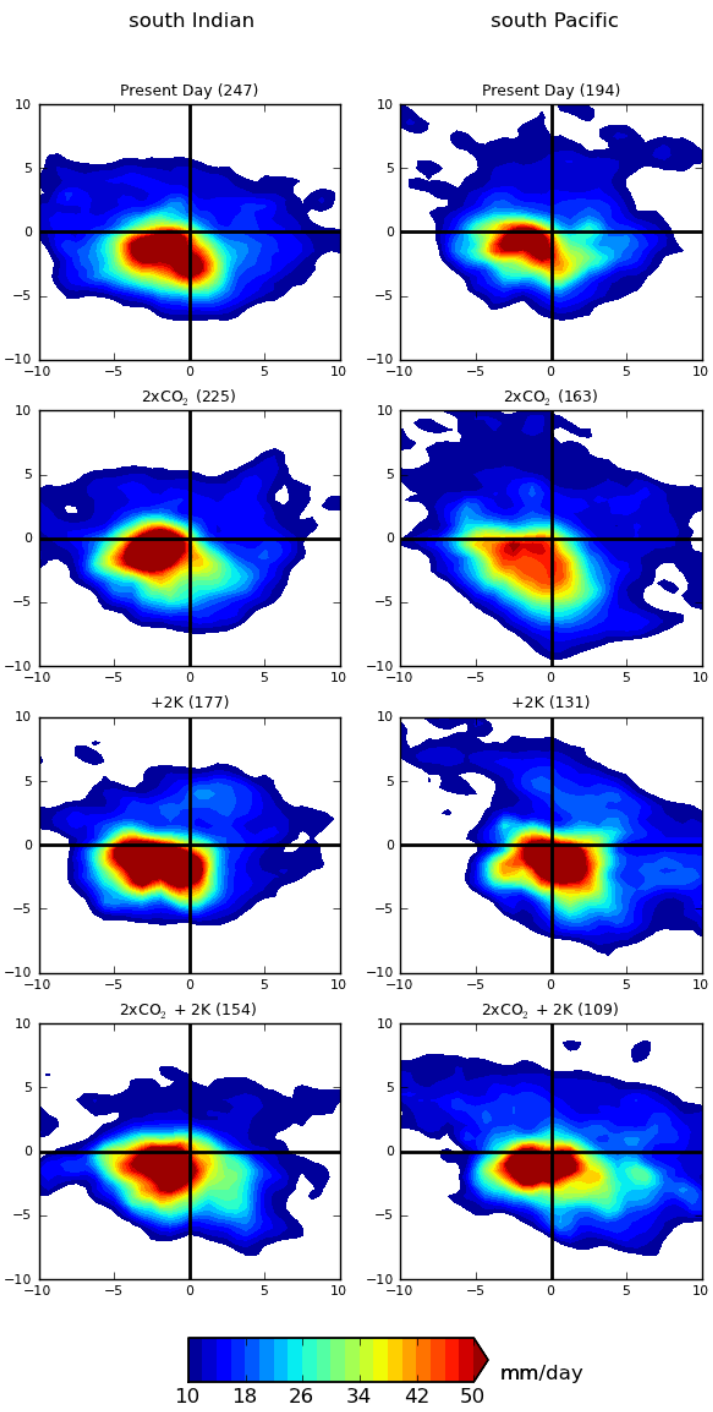

719

720 Figure 6: Composite mean daily rainfall patterns (in mm/day) for the storm days in the top-10%
721 rainiest TCs in the four GFDL simulations (rows) and in the two southern hemispheric TC basins
722 (columns). The number of TC storm days used in each composite is given in the panel titles, and
723 the x and y axes correspond to degrees from the TC center.

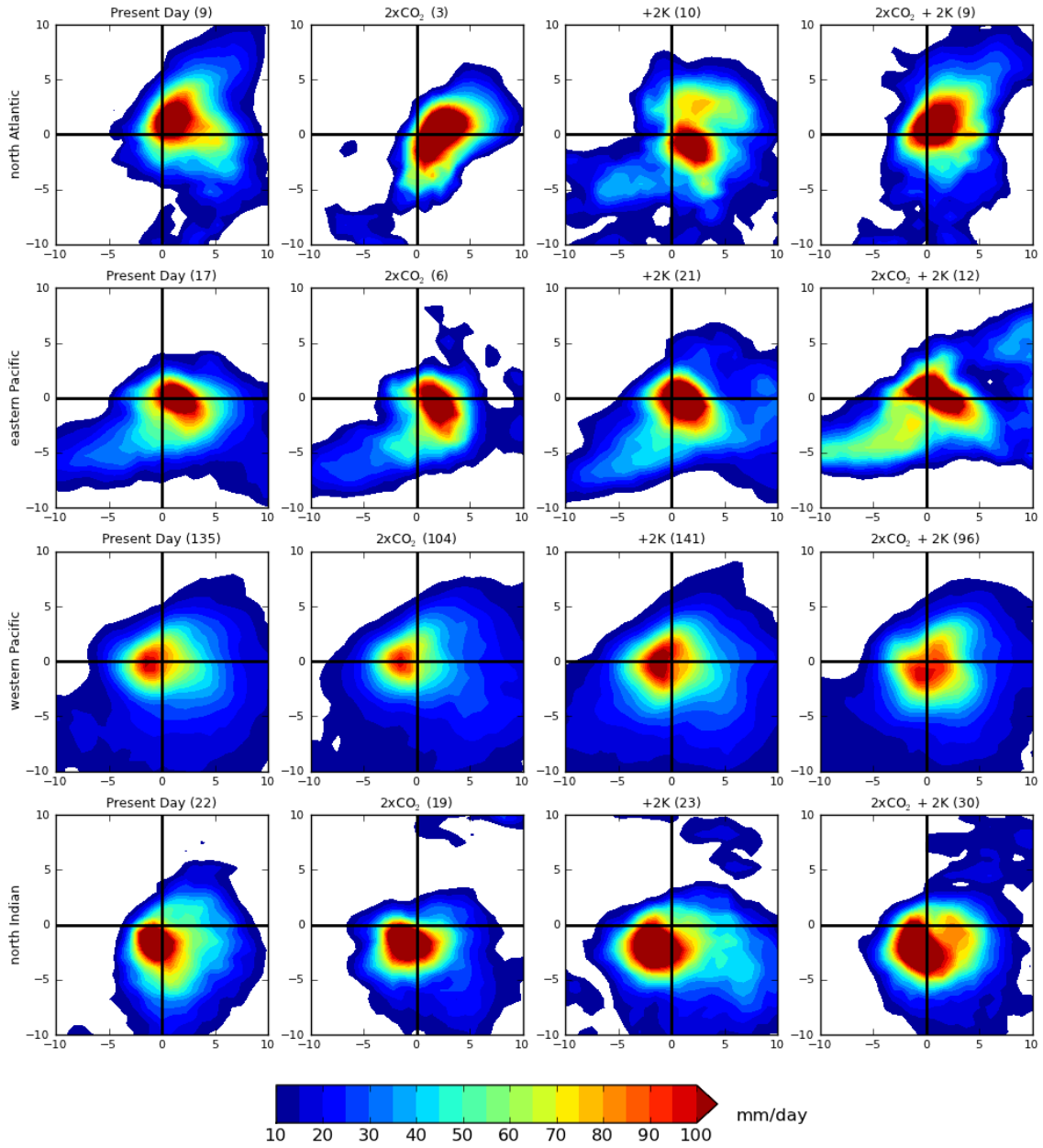

724

725 Figure 7: As in Figure 4, but for the CMCC model. Note that the color bar extends over twice the

726 range in Figure 4.

727

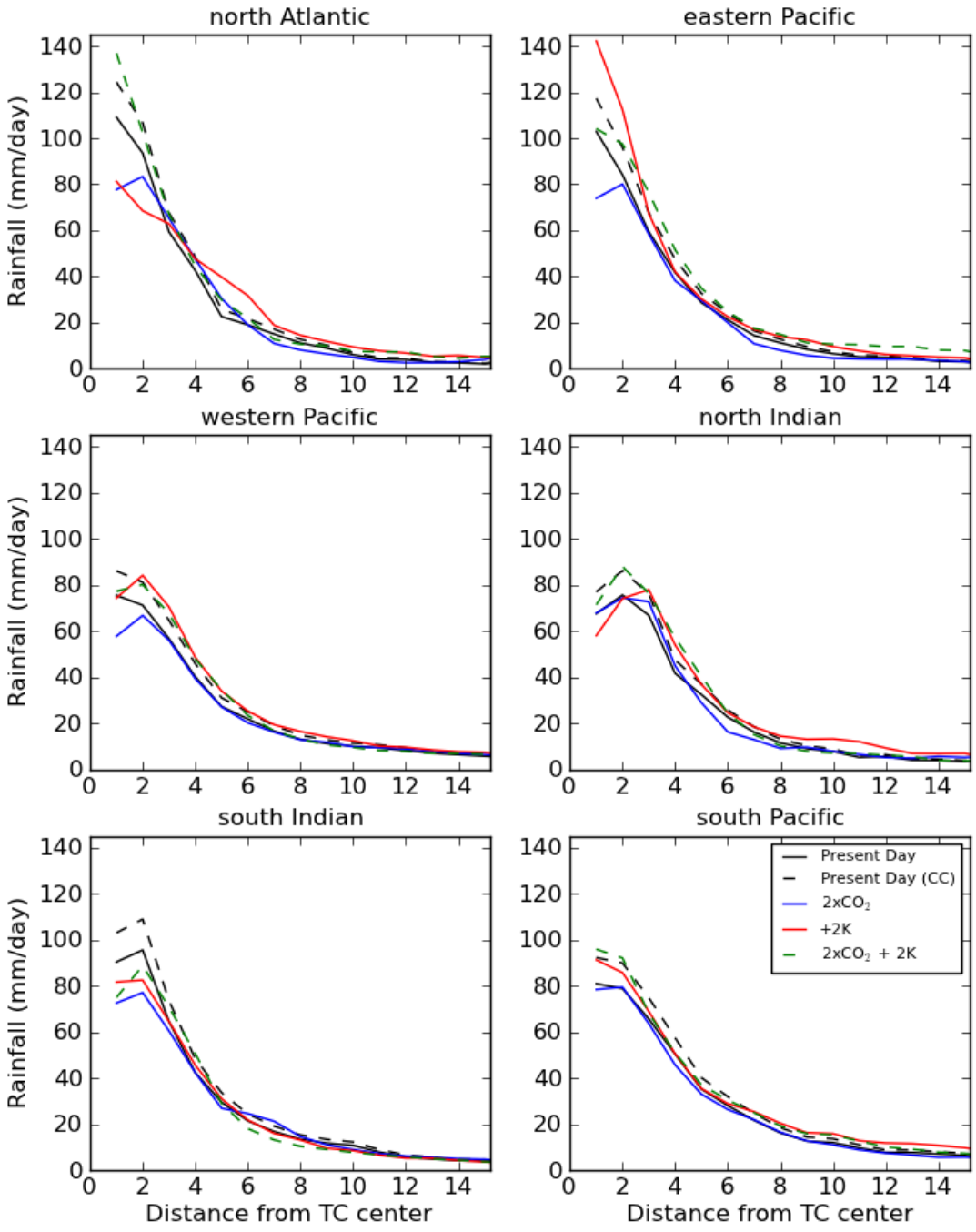

728

729 Figure 8: As in Figure 5, but for the CMCC model.

730

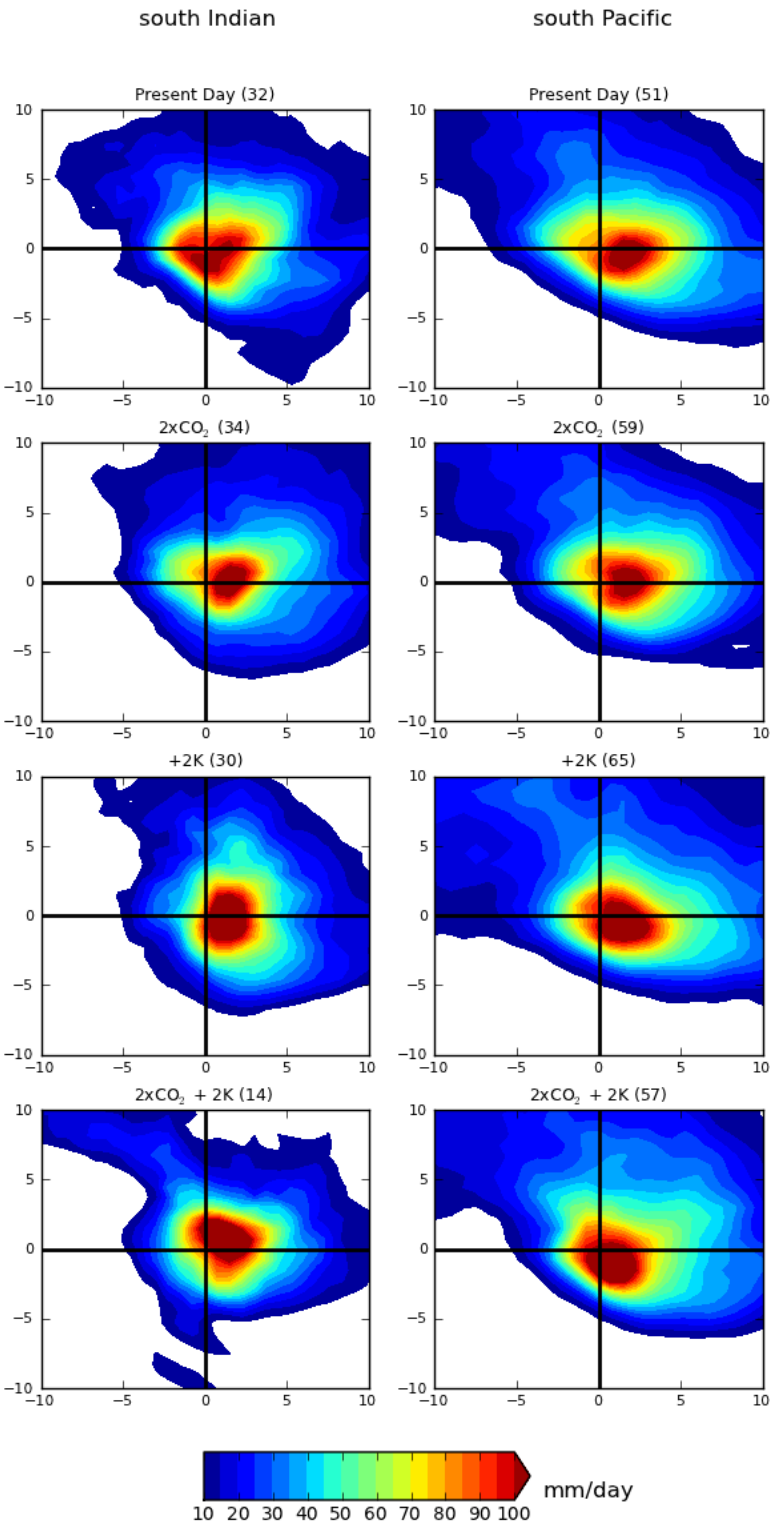

731

732 Figure 9: As in Figure 6, but for the CMCC model.

733

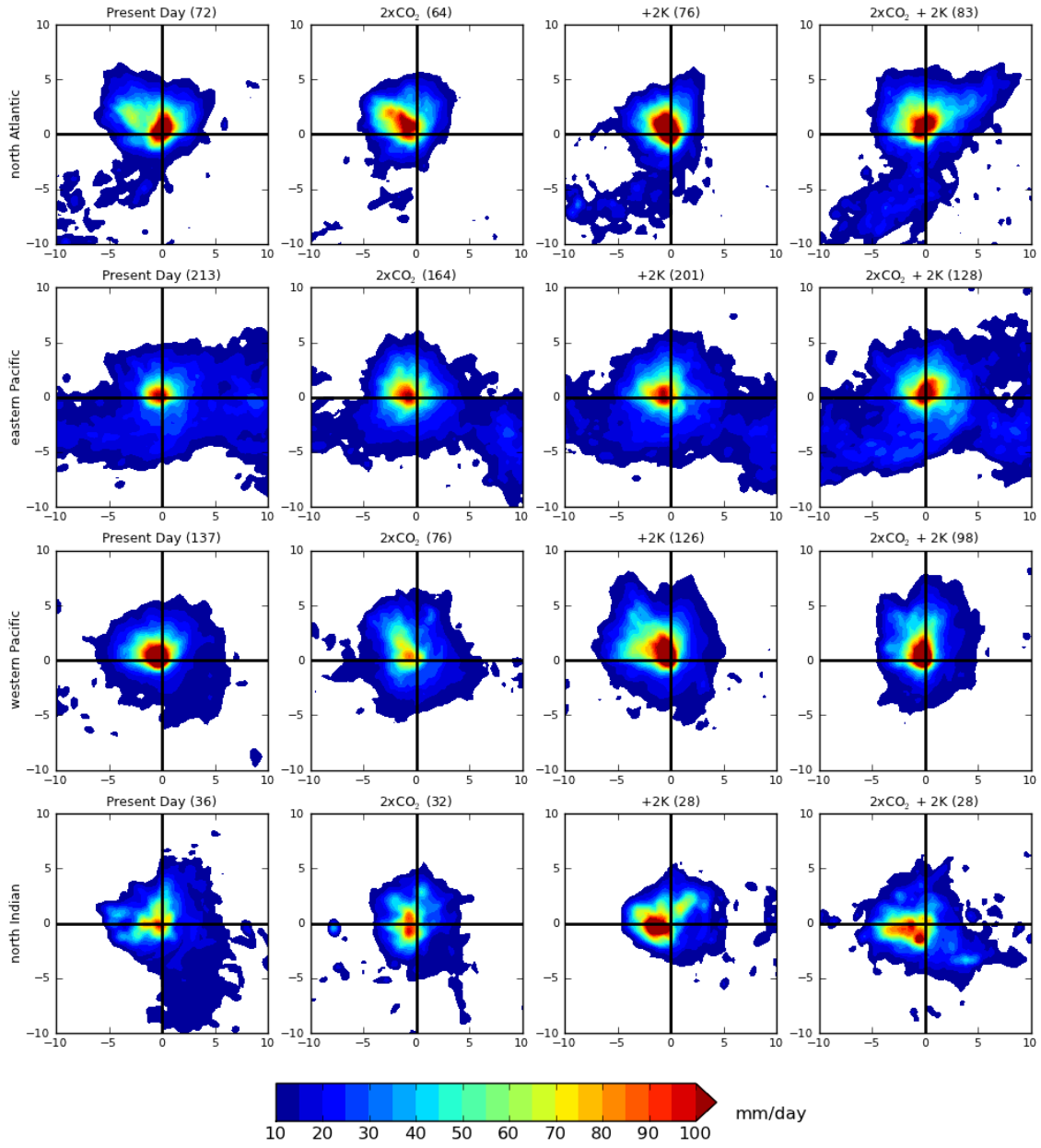

734

735

736 Figure 10: As in Figure 4, but for the CAM5 model. Note that the color bar extends over twice

737 the range in Figure 4.

738

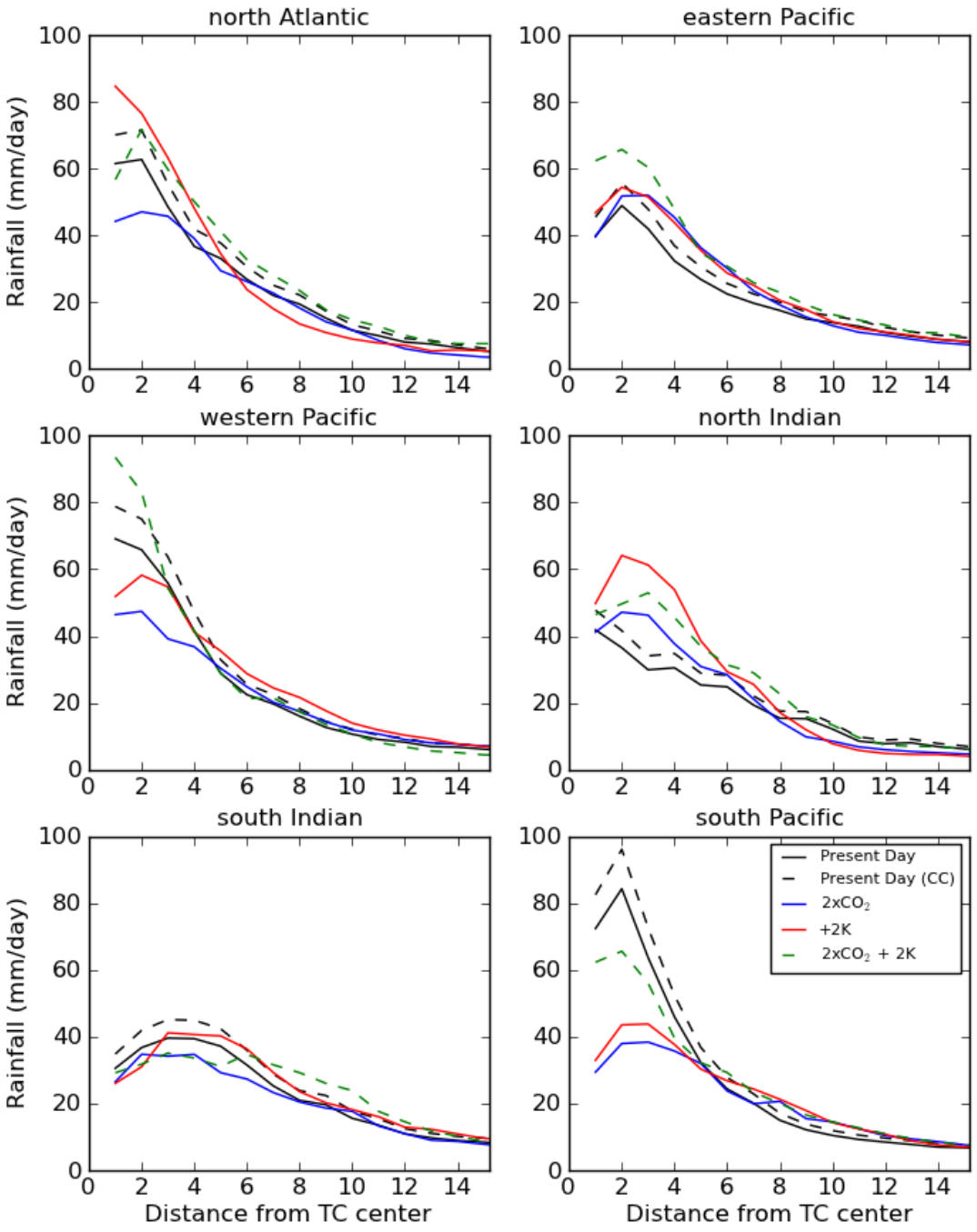

739

740 Figure 11: As in Figure 5, but for the CAM5 model. Note that 0.5° bins are used instead of the 1°

741 bins used in Figures 5 and 8.

742

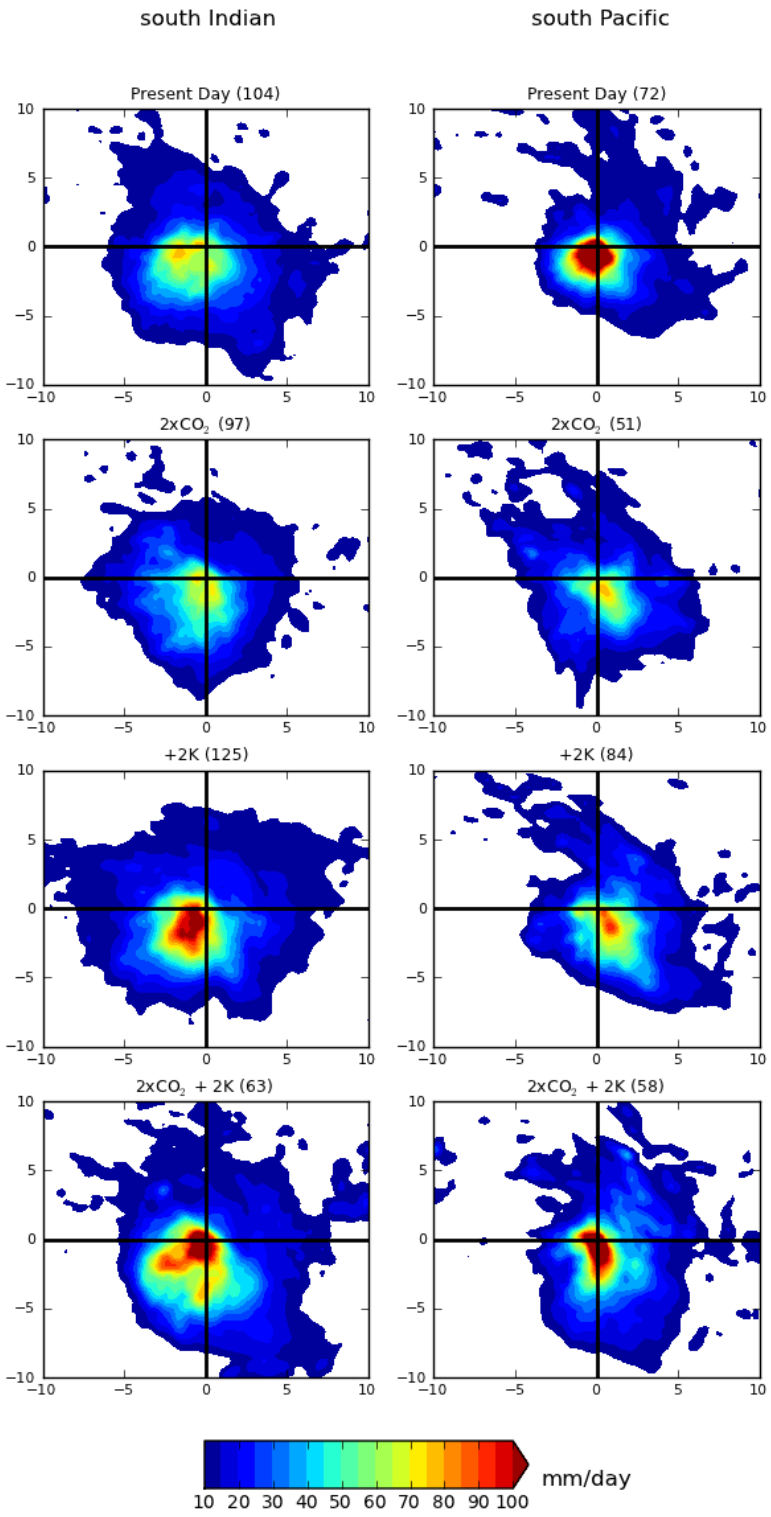

743

744 Figure 12: As in Figure 6, but for the CAM5 model.

745